CASSCF/6-31G* wave functions of **1** and **2** as the zeroth-order wave functions. Such correlated calculations are beyond the scope of the present investigation.

Regarding the activation barrier for the conversion of **1** into **2**, it should be noted that the value calculated at the CASSCF/6-31G* level is 5.3 kcal/mol higher than the calculated at the CASSCF/3-21G level. This result is consistent with the aforementioned fact that the 3-21G basis set overestimates the ring strain in **1**. Finally, at the highest level of theory employed in this investigation, namely, from the CASSCF/6-31G*//CASSCF/3-21G-calculated energies and the zero-point energy correction obtained from the CASSCF/3-21G-calculated vibrational frequencies, the activation barrier for the ring opening of **1** into **2** is predicted to be 21.9 kcal/mol, in excellent agreement with the experimental activation energies ranging from 19.1 to 22 kcal/mol.

## Conclusions

The following conclusions can be drawn from the ab initio UHF and CASSCF calculations reported here: (1) In qualitative agreement with early MINDO/3 calculations by Dewar and Kirschner, the thermal ring opening of **1** to give **2** takes place via a highly nonsymmetric transition state whose geometry shows unequal $C_1C_2$ and $C_1C_3$ bond lengths, with one methylene group having rotated $\sim 24°$ (relative to its position in **1**) whereas the other remains nearly orthogonal to the plane of the carbon atoms, the length of the CC undergoing rupture being $\sim 2$ Å.

(2) According to both the transition vector of this transition state and the IRC reaction path, the rotation of the second methylene group takes place in the last phase of the ring-opening process, namely, when the $C_2C_3$ bond is totally broken and the $C_1C_2$ $\pi$ bond is fully formed. This nonsynchronous rotation of the two methylene groups implies that the thermal conversion of **1** into **2** involves a common transition state for both the conrotatory and disrotatory modes of reaction. Therefore, in the absence of substituents in the methylene groups, which may lead to steric effects, there should be no special preference between the conrotatory and disrotatory modes. An experimental test of this interesting prediction is obviously highly desirable.

(3) In order to locate a transition structure for the ring opening of **1** into **2** it is necessary to use a MCSCF wave function whose CI expansion includes the singly excited configuration in which one electron is raised from the highest doubly occupied MO to the lowest unoccupied MO. This configuration appears to be essential to describe the electronic changes that take place at the transition state.

(4) Due to the substantial mixing of the $\langle S_z \rangle = +^1/_2$ component of the first quartet state into the UHF/3-21G doublet wave function, the latter method enables the calculation of a transition state for the ring opening of **1** into **2** whose geometry is similar to that found by using the CASSCF/3-21G model. Furthermore, the activation barrier calculated at the UHF/3-21G level differs only in 2.8 kcal/mol from that determined at the CASSCF/3-21G level. Therefore, the UHF/3-21G model is a good starting point to locate transition structures for the ring-opening reactions of cycloalkyl radicals.

**Acknowledgment**. This work was supported by the CICYT (Grant PB86-0270). The calculations were carried out with the IBM 4381 computer at the Centre d'Informàtica de la Universitat de Barcelona. We are indebted to Dr. Michael W. Schmidt (North Dakota State University) for providing us a copy of his greatly extended version of the GAMESS system of programs.

**Registry No. 1**, 2417-82-5; **2**, 1981-80-2.

**Supplementary Material Available:** Listing of Cartesian coordinates of the optimized molecular structures of **1**, TS, and **2**, calculated at the UHF/3-21G and CASSCF/3-21G levels of theory (3 pages). Ordering information is given on any current masthead page.

# Sustained Oscillations and Bistability in a Detailed Mechanism of the Peroxidase–Oxidase Reaction

**Baltazar D. Aguda and Raima Larter***

*Contribution from the Department of Chemistry, Indiana University–Purdue University at Indianapolis, Indianapolis, Indiana 46205.* *Received August 4, 1989*

**Abstract:** A detailed mechanism for the aerobic oxidation of NADH catalyzed by horseradish peroxidase, called the peroxidase–oxidase reaction, is studied by computer simulation and found to show bistability, damped and sustained oscillations. These oscillations are smooth and almost sinusoidal. The mechanism also predicts that a stable oscillatory state and a stable steady state can coexist for the same set of parameters. Decreasing the oxygen concentration in the gas phase for a short period of time is found to perturb the stable steady state toward the oscillatory state, while a spike of hydrogen peroxide drives an oscillatory state to a stable steady state. The mechanism is compared with detailed mechanisms proposed by other investigators as well as two 4-species abstract models we have studied previously.

## I. Introduction

Enzymes called peroxidases catalyze the oxidation of a large variety of organic substances using hydrogen peroxide. Because molecular oxygen can undergo a series of free radical reactions leading to hydrogen peroxide, some peroxidases can also catalyze the oxidation of a small number of hydrogen donors by oxygen. These hydrogen donors include nicotinamide adenine dinucleotide (NADH), nicotinamide adenine dinucleotide phosphate (NADPH), dihydroxyfumaric acid, indoleacetic acid, and triose reductone.[1] In this paper, we will only consider the peroxidase enzyme-catalyzed aerobic oxidation of NADH and refer to it as the peroxidase–oxidase (PO) reaction.[2] The stoichiometry of the overall reaction is

$$2NADH + O_2 + 2H^+ \rightarrow 2NAD^+ + 2H_2O \qquad (1)$$

When this reaction is carried out in an open system in which oxygen is continuously supplied to a well-stirred solution of NADH

(1) Olsen, L.; Degn, H. *Biochim. Biophys. Acta* **1978**, *523*, 321.
(2) Degn, H.; Olsen, L.; Perram, J. *Ann. N.Y. Acad. Sci.* **1979**, *316*, 623.

0002-7863/90/1512-2167$02.50/0 

**Table I.** Observed Nonlinear Behaviors of the Peroxidase–Oxidase Reaction in an Open System

| behavior | investigators | exptl conditions[a] |
|---|---|---|
| A. damped oscillations | Yamazaki, Yokota, and Nakajima, 1965 (ref 41) | pH 5.12, 25 °C, $O_2/N_2$ (1:24) bubbled, 0.8 mM NADH, 10 μM HRP |
| B. bistability | Degn, 1968 (ref 17) | pH 5.5, 25 °C, $O_2/N_2$ blown, 1.4 mM NADH, 0.4 μM HRP |
| C. sustained oscillations | Nakamura, Yokota, and Yamazaki, 1969 (ref 3) | pH 6.4, 25 °C, 5% $O_2$ bubbled, 1 mM NADPH, 10 μM HRP, added: glucose-6-phosphate dehydrogenase, methylene blue, and 2,4-dichlorophenol |
| D. chaos | Olsen and Degn, 1977 (ref 40) | pH 5.1, 28 °C, 1.65% $O_2$ blown, infusion of 0.25 mM NADH, 1.2 μM HRP, added: methylene blue and 2,4-dichlorophenol |

[a] HRP = horseradish peroxidase. No infusion of NADH in A and B.

**Table II.** Reactions Involved in the Peroxidase–Oxidase System and Their Rate Constants

| no. | reaction | reaction rate, $v$ | rate const, $k$ | ref |
|---|---|---|---|---|
| $R_1$ | $Per^{3+} + H_2O_2 \rightarrow$ col | $k_1[Per^{3+}][H_2O_2]$ | $1.8 \times 10^7$ $M^{-1}$ $s^{-1}$ | 1, 4, 26–29 |
| $R_2$ | col + NADH → colI + NAD• | $k_2$[col][NADH] | $5.4 \times 10^3$ $M^{-1}$ $s^{-1}$ | 4, 26–28 |
| $R_3$ | colI + NADH → $Per^{3+}$ + NAD• | $k_3$[colI][NADH] | $8.0 \times 10^2$ $M^{-1}$ $s^{-1}$ | 26–28 |
| $R_4$ | colI + $H_2O_2$ → colII | $k_4$[colI][$H_2O_2$] | 46.0 $M^{-1}$ $s^{-1}$ | 30 |
| $R_{-4}$ | colII → colI + $H_2O_2$ | $k_{-4}$[colII] | $2.0 \times 10^{-3}$ $s^{-1}$ | 31 |
| | | | $3.0 \times 10^{-4}$ $s^{-1}$ | 4 |
| $R_5$ | $Per^{3+}$ + NAD• → $Per^{2+}$ + $NAD^+$ | $k_5[Per^{3+}]$[NAD•] | very slow | 4, 32 |
| $R_6$ | $Per^{2+}$ + $O_2$ → colII | $k_6[Per^{2+}][O_2]$ | $5.8 \times 10^4$ $M^{-1}$ $s^{-1}$ | 32, 33 |
| $R_7$ | colII + NADH → col + NAD• + $H^+$ | $k_7$[colII][NADH] | very slow | 34, 35 |
| $R_8$ | colII + NAD• → col + $NAD^+$ | $k_8$[colII][NAD•] | $1.3 \times 10^8$ $M^{-1}$ $s^{-1}$ | 4, 35 |
| $R_9$ | col + $O_2^-$ → colI + $O_2$ | $k_9$[col][$O_2^-$] | | 36 |
| $R_{10}$ | $Per^{3+}$ + $O_2^-$ → colII | $k_{10}[Per^{3+}][O_2^-]$ | $1.9 \times 10^6$ $M^{-1}$ $s^{-1}$ | 4, 32, 37 |
| | | | $1.5 \times 10^5$ $M^{-1}$ $s^{-1}$ | 5 |
| $R_{11}$ | NAD• + $O_2$ → $NAD^+$ + $O_2^-$ | $k_{11}$[NAD•][$O_2$] | $2.0 \times 10^9$ $M^{-1}$ $s^{-1}$ | 4, 19, 32 |
| $R_{12}$ | $H^+$ + $O_2^-$ + NADH → $H_2O_2$ + NAD• | $k_{12}[O_2^-]$[NADH] | $5.9 \times 10^3$ $M^{-1}$ $s^{-1}$ | 4, 32 |
| | | | $<3.5 \times 10^4$ $M^{-1}$ $s^{-1}$ | 5 |
| $R_{13a}$ | 2NAD• + $H^+$ → NADH + $NAD^+$ | $k_{13a}$[NAD•]$^2$ | | 32 |
| $R_{13b}$ | 2NAD• → NAD–NAD | $k_{13b}$[NAD•]$^2$ | $3.0 \times 10^7$ $M^{-1}$ $s^{-1}$ | 18, 19 |
| $R_{14}$ | $2O_2^-$ + $2H^+$ → $H_2O_2$ + $O_2$ | $k_{14}[O_2^-]^2$ | $1.1 \times 10^7$ $M^{-1}$ $s^{-1}$ | 32, 38 |
| | | | $2.0 \times 10^7$ $M^{-1}$ $s^{-1}$ | 5 |
| $R_{15}$ | $Per^{2+}$ + colII → $Per^{3+}$ + col | $k_{15}[Per^{2+}]$[colII] | very fast | 4, 33, 39 |
| $R_{16}$ | NADH + $O_2$ + $H^+$ → $H_2O_2$ + $NAD^+$ | $k_{16}$[NADH][$O_2$] | $3.0 \times 10^{-6}$ $s^{-1}$ | 4, 35 |
| $R_{17}$ | NAD• + $H_2O_2$ + $H^+$ → $NAD^+$ + $H_2O$ + HO• | $k_{17}$[NAD•][$H_2O_2$] | $8.6 \times 10^8$ $M^{-1}$ $s^{-1}$ | 4 |
| $R_{18}$ | NADH + HO• → NAD• + $H_2O$ | $k_{18}$[NADH][HO•] | | 4 |

and horseradish peroxidase, a variety of nonlinear behavior is observed including bistability, damped and sustained oscillations, and chaos.[2] The first reported observations of these phenomena are listed in Table I. Sustained oscillations were first observed in a related reaction involving NADPH as the substrate; in this system, NADPH is kept at a constant level by regenerating it from its oxidation product with a second enzyme glucose-6-phosphate dehydrogenase.[3] Experiments[1] wherein NADH is pumped into the solution at a constant rate (instead of regenerating it with an enzyme reaction as was done for NADPH) have yielded stable periodic oscillations as well.

Analyses of some proposed mechanisms for the PO reaction have been performed by Yokota and Yamazaki[4] (closed system), Olsen and Degn,[1,5] and Fed'kina and co-workers[6,7] (closed and open systems). Fed'kina, Ataullakhanov, and Bronnikova[7] have presented computer simulations using a detailed mechanism which, in a reduced form derived by applying several restrictive assumptions, generated sustained oscillations. Using the stoichiometric network analysis formalism,[8] Aguda and Clarke[9] studied a large network of reactions consisting of known possible mechanistic steps and were able to identify the steady state pathways and feedback loops that are dominant under bistable conditions. On the basis of these dominant pathways, they proposed a model that was shown to exhibit bistability and damped oscillations, among other things; we shall refer to this latter mechanism as model A. The main purpose of this paper is to show that model A is also sufficient to account for the sustained oscillations exhibited by the PO reaction in some laboratory experiments. A secondary purpose is to elucidate the source of the oscillatory behavior in terms of the interaction of the feedback loops present in the mechanism.

We discuss in section II some background concerning experimental details of the PO reaction and summarize the results and problems of previous modeling studies of the reaction. Also in section II, we point out some similarities between two 4-species models[2,10] we have studied previously and the detailed mechanism, model A, studied here. Our previous studies[11-13] of the simple 4-species models have helped us considerably in developing some intuitive understanding of the dynamics of the PO reaction. New computational results for model A are given in section III. There it is shown that model A also exhibits bistability between a stable oscillatory state and a stable steady state for some choices of rate constants and total enzyme concentration. Previously, Aguda and Clarke[9] have only found bistability between two stable steady states in model A, so the results reported here constitute a significant advance in our understanding of the details of the biochemistry which lead to sustained oscillatory behavior in the PO reaction.

## II. The Peroxidase–Oxidase Mechanism

We will review in this section some of the detailed mechanisms that have been previously proposed for the PO reaction. A listing of possible reactions involved in the PO mechanism is given in Table II along with available values of the rate constants, either extracted from experimental data or derived from computer simulations. The following standard abbreviations have been used

(3) Nakamura, S.; Yokota, K.; Yamazaki, I. *Nature* **1969**, *222*, 794.
(4) Yokota, K.; Yamazaki, I. *Biochemistry* **1977**, *16*, 1913.
(5) Olsen, L. *Biochim. Biophys. Acta* **1978**, *527*, 212.
(6) Fed'kina, V.; Ataullakhanov, F.; Bronnikova, T.; Balabaev, N. *Biophys. Chem.* **1978**, *72*, 195.
(7) Fed'kina, V.; Ataullakhanov, F.; Bronnikova, T. *Biophys. Chem.* **1984**, *19*, 259.
(8) Clarke, B. L. *Adv. Chem. Phys.* **1980**, *43*, 1.
(9) Aguda, B. D.; Clarke, B. L. *J. Chem. Phys.* **1987**, *87*, 3461.
(10) Olsen, L. *Phys. Lett.* **1983**, *A94*, 454.
(11) Larter, R.; Bush, C.; Lonis, T.; Aguda, B. *J. Chem. Phys.* **1987**, *87*, 5765.
(12) Larter, R.; Steinmetz, C.; Aguda, B. *J. Chem. Phys.* **1988**, *89*, 6506.
(13) Aguda, B. D.; Larter, R.; Clarke, B. *J. Chem. Phys.* **1989**, *90*, 4168.

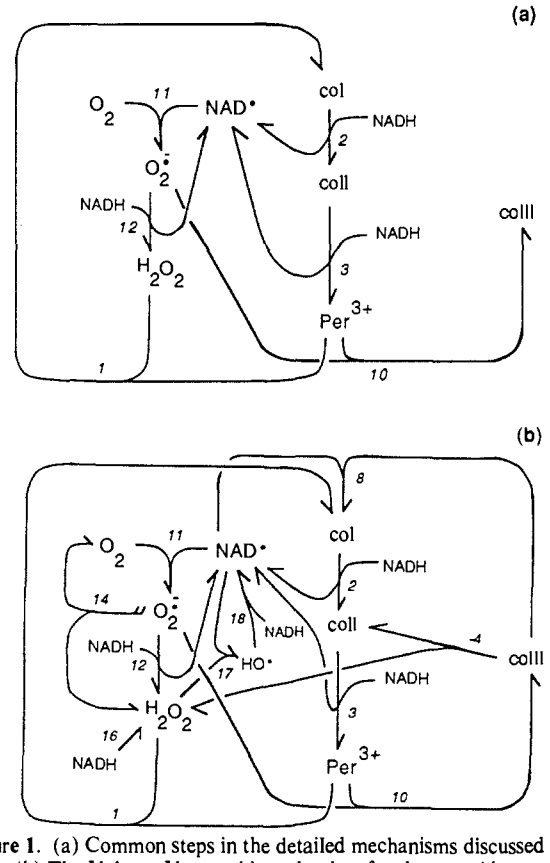


**Figure 1.** (a) Common steps in the detailed mechanisms discussed in the text. (b) The Yokota–Yamazaki mechanism for the peroxidase–oxidase reaction. See Table II for the details of the reaction steps. For each reaction arrow, the number of barbs on the arrow head gives the number of molecules of product formed and the number of feathers on the left side of the arrow tail gives the order of kinetics with respect to the given reactant species. (This convention is adopted from Clarke, ref 8.)

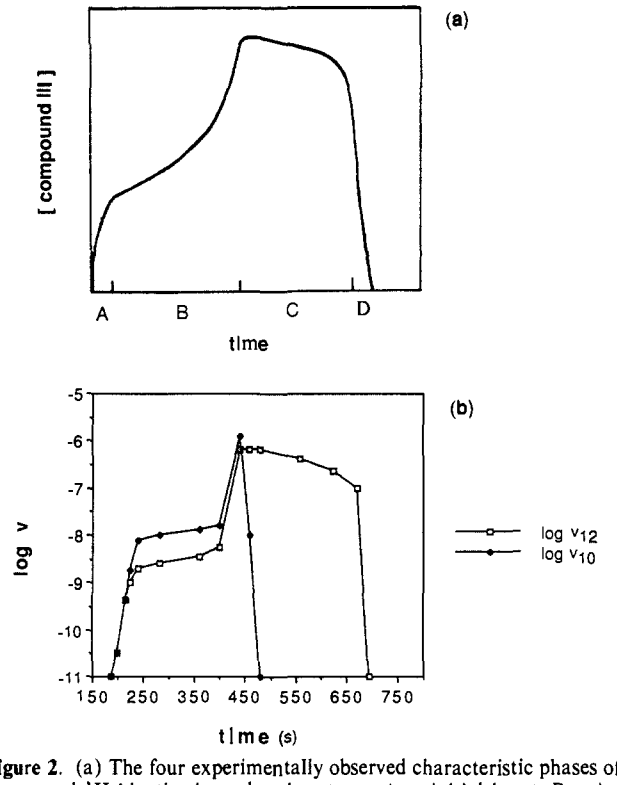


**Figure 2.** (a) The four experimentally observed characteristic phases of compound III kinetics in a closed system: A = initial burst, B = induction, C = steady state, and D = abrupt decomposition. (b) Corresponding logarithm of the rates of reactions $R_{10}$ and $R_{12}$ during the four phases of compound III kinetics.

in Table II for the five enzyme species (listed here in order of increasing oxidation state, +2 to +6): $Per^{2+}$ = ferroperoxidase, $Per^{3+}$ = ferriperoxidase (native enzyme), coII = compound II, col = compound I, and coIII = compound III.

The reactions shown in Figure 1a are common to all the mechanisms discussed below. The differences between these mechanisms reflect the uncertainties in the way compound III decomposes. Note that the feedback loop composed of reactions $R_1$, $R_2$, and $R_3$ represents the peroxidase catalytic cycle that generates NAD• free radicals. Adding reactions for the decomposition of compound III will introduce another feedback cycle that would be coupled to the peroxidase catalytic cycle. As shown in Figure 1, the branching steps leading separately to the two feedback loops are the reactions $R_{10}$ and $R_{12}$. The interaction between these two feedback loops generates interesting dynamics when oxygen and/or NADH are fed continuously into the open system.

**A. The Yokota–Yamazaki (YY) Mechanism.** A computer simulation of a detailed mechanism of the PO reaction in a closed system was performed by Yokota and Yamazaki (YY).[4] The YY reaction scheme includes the steps shown in Figure 1a and reactions $R_8$, $R_{-4}$, $R_{14}$, $R_{16}$, $R_{17}$, and $R_{18}$ found in Table II; Figure 1b shows the network diagram of the YY scheme. Note that the bimolecular reaction between compound III and NAD• radical is considered to be the dominant decomposition pathway for compound III in the YY mechanism. The reactions involving the enzyme species $Per^{2+}$ are not considered in the YY scheme.

In their computer simulations, YY used reported experimental values of the rate constants available at that time and were able to generate the four experimentally observed characteristic phases of compound III kinetics shown in Figure 2a: initial burst, induction, steady state, and abrupt decomposition. The YY simulations reproduce these four phases nearly quantitatively. Aguda[14] confirmed their simulations and also showed that the time series for the concentrations of $O_2$, NADH, $H_2O_2$, coII, and coIII have the same qualitative appearance as those observed experimentally.

A clue as to why oscillations are observed when the system is continuously "pumped" with oxygen and NADH can be gleaned from the variation in reaction velocities through the four characteristic phases. As shown in Figure 2b, the velocities of the two branching reactions, $R_{10}$ and $R_{12}$, increase in a similar fashion during the induction phase (i.e. when molecular oxygen is not being consumed because of a low level of NAD•). However, the rate of coIII formation ($v_{10}$) drops drastically during the transition from the induction phase to the steady-state phase because of the depletion of $Per^{3+}$. CoIII attains a near-steady-state level because not enough NAD• radicals are present to transform it into CoI via reaction $R_8$. In the meantime, the catalytic cycle initiated by the branching reaction $R_{12}$ generates these NAD• radicals that will eventually break down coIII. When oxygen is depleted, the decomposition of coIII through its reaction with NAD• radicals gets accelerated due to the production of more radicals by reactions $R_2$ and $R_3$. With a continuous input of oxygen, this cycle (i.e. increase in coIII followed by an increase in NAD• radicals which causes the decomposition of coIII) can be sustained.

Even though the results of simulations with the YY mechanism agree very well with experiment, we must caution that certain mathematical inconsistencies exist in the YY kinetic equations that may render the conclusions questionable. First, they used the rate expression $v_{16} = k_{16}[NADH]$ for the autoxidation reaction of NADH ($R_{16}$) but neither the expression for d[NADH]/d$t$ nor that for d[$O_2$]/d$t$ involves $v_{16}$. Second, YY added reactions $R_{17}$ and $R_{18}$ (cancelling NAD• and HO• radicals) and used the rate expression $v_{17} = k_{17}[NAD•][H_2O_2]$ for the combined reaction; although $v_{17}$ does not contain [NADH] as a factor, the expression for d[NADH]/d$t$ does include the negative term ($-v_{17}$) which could possibly drive [NADH] down to negative values. Lastly, the YY scheme does not contain a chain terminating reaction like $R_{13}$ (in Table II), and this is probably the reason why a significant

(14) Aguda, B. D. Unpublished Notes, 1985.

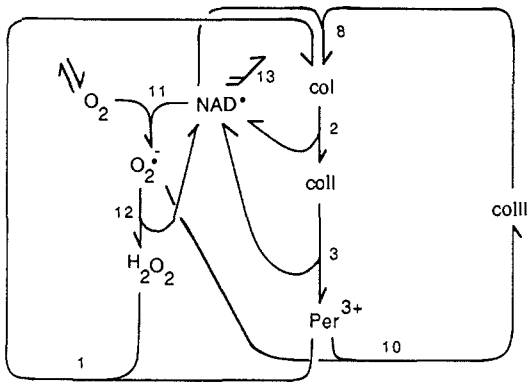


**Figure 3.** Network diagram of model A for the peroxidase–oxidase reaction. The details of the component reactions are given in Table II.

amount of NAD• radicals are present at the end of the reaction as was found by Aguda[14] when he duplicated the YY computer simulations.

**B. The Fed'kina–Ataullakhanov–Bronnikova (FAB) Oscillatory Mechanism.** The FAB mechanism[7] consists of those common reactions in Figure 1a, reaction $R_8$ (Table II), and a termination reaction of NAD• radicals which is first order in [NAD•]. It is, in fact, identical with the next model to be discussed below (model A, shown in Figure 3) except for the order of the termination reaction for NAD• radicals. Second-order termination kinetics, which is the case for model A, is necessary for the existence of three steady states for the open reaction system.[15]

The FAB simulations were performed under the following assumptions: NADH is kept at constant concentration; compounds I, II, and III and $O_2^-$ are fast variables that relax rapidly to the slow motion of the system described by the differential equations involving NAD•, $H_2O_2$, and $O_2$; and finally, $O_2$ changes in a quasistationary manner at the characteristic time of the slow subsystem. Under these restrictive assumptions, oscillations are then found in the concentrations of the two remaining dynamical species, NAD• and $H_2O_2$. As in the YY scheme, $Per^{2+}$ is ignored in the FAB mechanism.

FAB reported an expression (eq 4 in ref 7) for the period of the oscillations as a function of total enzyme concentration ($E_t$), NADH concentration, and the rate constants associated with the reactions of the feedback loop involving coIII. This expression predicts that the oscillation period increases with $E_t$ in a hyperbolic manner, Although Fed'kina and co-workers[16] have demonstrated experimentally that smooth (instead of the usual sawtooth[2]) oscillations do indeed occur by raising the temperature, it was also observed that (at low oxygen concentrations) decreasing $E_t$ leads to an increase in the oscillation period which is contrary to the FAB expression mentioned above,

**C. A Bistable Mechanism; Model A.** Using stoichiometric network analysis,[8] Aguda and Clarke[9] extracted a bistable model from the reactions listed in Table II, This mechanism, referred to as model A, is shown in Figure 3. Note that it differs from the FAB mechanism only in the bimolecular termination reaction for NAD• radical. Model A was shown to have the same network components responsible for the bistability exhibited by the 4-species classical substrate-inhibition enzyme mechanism.[17] These network components necessary for bistability are the following: a catalytic cycle coupled with an inhibition cycle, and a reversible flux of substrate.

Model A was previously shown to exhibit bistability, damped oscillations, and substrate inhibition.[9] Our computer simulations using this model will be presented in the next section where we show that it generates sustained oscillations as well. In contrast to the study of the FAB mechanism, we do not reduce the kinetic equations by assuming any fast or slow variables but, rather, we integrate the whole set of differential equations. Note that pH and NADH concentration are kept constant, and $Per^{2+}$ is excluded as in the YY and FAB schemes.

**D. Other Models and Features of the PO Mechanism.** The reported value for the rate constant of the reaction between $Per^{2+}$ and $O_2$ ($R_6$ in Table II) is just a few orders of magnitude smaller than that of the reaction between NAD• radicals and $O_2$ ($R_{11}$ in Table II), and $Per^{2+}$ probably should be included in a detailed model, The three models discussed above ignored reactions involving $Per^{2+}$ mainly because this enzyme species is known to be produced very slowly by the reaction between $Per^{3+}$ and NAD• radicals ($R_5$ in Table II) so its concentration is not high. A model that included $Per^{2+}$ (model I of Fed'kina et al.[6]) did not agree with the experimental observation[16] that as the initial oxygen concentration is increased, the duration of the induction phase lengthens. Fed'kina and co-workers[6] showed that model I predicts exactly the opposite. However, in agreement with experiments, model I does predict that the duration of the steady-state phase increases with initial oxygen concentration. Fed'kina et al.[6] studied another model similar to the YY scheme which predicts that the duration of the induction phase does not depend on the initial concentration of oxygen; however, this same model does agree with experiment regarding the duration of the steady-state phase.

Reaction $R_{11}$ is a step in which oxygen directly drives the two feedback loops in the mechanism. Another reaction that could drive the feedback loop involving compound III is reaction $R_6$ between oxygen and $Per^{2+}$ which is not included in model A. As will be discussed in the next subsection, an analogous 4-species model in which two coupled feedback loops are both driven by oxygen can give rise to complex mixed-mode oscillations. The role of reaction $R_6$ in generating mixed-mode oscillations in the detailed mechanism will be investigated in a future publication.

Another complicating feature of the PO mechanism is the role of $(NAD)_2$ dimers, The rate constant for the dimerization of NAD• radicals has been reported to be about $3 \times 10^7$ $M^{-1}$ $s^{-1}$, and this reaction may be the preferred route for NAD• chain termination rather than the disproportionation of NAD• radicals.[18,19] Avigliano and co-workers[20] have shown that horseradish peroxidase catalyzes the oxidation of $(NAD)_2$ dimers to $NAD^+$ and postulated some reaction schemes in which the dimer reacts in a similar fashion as NADH. Again, these points are not taken into account in model A but should be considered in future refinements of the detailed mechanism.

Lastly, but probably not the least important, the mechanistic roles played by dichlorophenol and methylene blue in the sustained oscillations need to be elucidated (see Table I). Olsen and Degn[1] report that dichlorophenol must be present in order to obtain sustained oscillations, otherwise only damped oscillations are observed. It is observed that addition of dichlorophenol causes a rapid decrease in the concentrations of oxygen and coIII. Furthermore, the bistability phenomenon disappears with the addition of dichlorophenol.[1] On the other hand, methylene blue is not required for sustained oscillations but is useful to stabilize these oscillations under certain conditions.

**E. Abstract Models of the PO Reaction.** Degn, Olsen, and Perram (DOP)[2] proposed a 4-species model that can simulate the experimentally observed sustained sawtooth oscillations of the PO reaction. This model is shown in Figure 4a. Species A is assumed to be oxygen, B is NADH, and X and Y are unidentified chain carrier species involved in autocatalytic reactions. Later, Olsen[10] proposed a very similar model shown in Figure 4b. Both the DOP and Olsen models show chaotic oscillations,[11-13] as was known experimentally, but the latter model has been shown to generate chaos within a broader range of some parameters.[10,13] We have also found mixed-mode oscillations in both models[11,13] as well as quasiperiodicity and phase-locking on a torus in the DOP model;[21]

(15) Aguda, B. D. Ph.D. Thesis, University of Alberta, 1986.
(16) Fed'kina, V.; Bronnikova, T.; Ataullakhanov, F. *Stud. Biophys.* **1981**, *82*, 159.
(17) Degn, H. *Nature* **1968**, *217*, 1047.
(18) Samec, Z.; Bresnahan, W. T.; Elving, P. J. *J. Electroanal. Chem.* **1982**, *133*, 1.
(19) Land, E. J.; Swallow, A. J. *Biochim. Biophys. Acta* **1971**, *234*, 34.
(20) Avigliano, L.; Carelli, V.; Casini, A.; Finazzi-Agro, A.; Liberatore, F. *Biochem. J.* **1985**, *226*, 391.
(21) Steinmetz, C.; Larter, R.; Aguda, B. *Proc. Indiana Acad. Sci.*, in press.

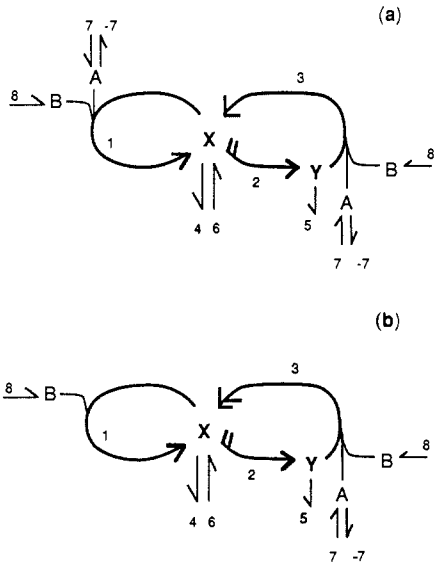


**Figure 4.** (a) The Degn-Olsen-Perram model (ref 2) for the peroxidase-oxidase reaction. (b) The Olsen model (ref 10) for the peroxidase-oxidase reaction. In both models, A = $[O_2]$, B = [NADH], and X and Y are chain carrier intermediates.

neither of these behaviors has yet been confirmed experimentally.

In a recent paper,[13] we showed that the intermediate X plays the same role as NAD• and species Y the same role as compound III in a more realistic mechanism such as model A. Here we point out the similarities between the two feedback loops present in both the 4-species models and the realistic mechanism. The autocatalytic reaction 1 (of the 4-species models) corresponds to the peroxidase catalytic cycle that generates NAD• radicals. The other feedback loop involving Y and reactions 2 and 3 (of the 4-species models) corresponds to the enzyme feedback loop that involves compound III. Simulations with the Olsen model performed previously[13] showed that when the rate constant for the production of Y is low, only damped oscillations are observed; likewise, if the rate constant for compound III production is not sufficiently high, only damped oscillations are found.[7,13] Our previous experience with these four-species models in fact guided us in finding values of the rate constants that produced sustained oscillations in model A.

We also see that in the Olsen model, the reaction involving A (oxygen) is linked only to the feedback loop involving Y. This corresponds, in a realistic mechanism, to the reaction between ferroperoxidase and oxygen (not included in model A) which produces compound III, thus entering the second feedback loop. The DOP model, in contrast, has oxygen entering both feedback loops; correspondingly, in the detailed mechanism, the reaction between oxygen and NAD• ($R_{11}$) drives both feedback loops via the branching reactions $R_{10}$ and $R_{12}$. In this respect, the DOP model may be in better agreement with the realistic mechanism than the Olsen model.

Simulations of the detailed PO mechanisms have so far not yielded the complex oscillations or chaos seen in the experiments and simulations with the 4-species models. We believe that the "forcing" of the feedback loops by species A (oxygen) is responsible for these behaviors in the 4-species models[11-13] and that complex oscillations and chaos will not be observed in these detailed mechanisms unless a similar forcing reaction is included. Toward this goal, the effect of including the reaction between $Per^{2+}$ and $O_2$ ($R_6$ in Table II) as a step forcing the feedback loop involving coIII is currently being studied by our group.

## III. Results of Computer Simulations with Model A

**A. Dynamical Equations.** Assuming isothermal and well-stirred conditions, the kinetics of the reaction system is given by the following set of autonomous ordinary differential equations

$$d\mathbf{X}/dt = \nu\mathbf{v}(\mathbf{X},\mathbf{k}) \qquad (2)$$

where $\mathbf{X}$ is a vector of $n$ concentrations, $\mathbf{v}$ is a vector of $r$ reaction rates that are functions of $\mathbf{X}$ and the vector of rate constants $\mathbf{k}$, and $\nu$ is the $nxr$ stoichiometric matrix whose element $\nu_{ij}$ is equal to the stoichiometric coefficient of species $X_i$ on the product side minus that on the reactant side of reaction $R_j$.

For model A, $n = 8$ and $r = 10$ and we let $\mathbf{X} = ([H_2O_2]$, [NAD•], $[O_2^-]$, $[O_2]$, $[Per^{3+}]$, [coI], [coII], [coIII]) where [ ] indicates "concentration of". Only 7 of the 8 species are independent dynamical variables because of the conservation of total enzyme concentration, i.e.

$$E_t = [Per^{3+}] + [coI] + [coII] + [coIII] = \text{constant} \qquad (3)$$

Thus, we have a total of 11 parameters (10 rate constants and 1 conservation constraint) in the dynamical equations of model A.

The components of the vector of reaction rates, $\mathbf{v} = (v_1, v_2, v_3, v_8, v_{10}, v_{11}, v_{12}, v_{13}, v_{in}, v_{out})$, are given in the third column of Table II ($v_{in}$ and $v_{out}$ are defined below). Recall that NADH is not a dynamical species so that either reaction $R_{13a}$ or $R_{13b}$ in Table II can be chosen. The rates $v_{in}$ and $v_{out}$ correspond to the two terms in the rate of diffusion of oxygen gas across the phase boundary (see ref 2) as given by the following expression

$$\text{diffusion rate} = k_t([O_2]_{eq}-[O_2]) = v_{in} - v_{out} \qquad (4)$$

where $[O_2]_{eq}$ is the dissolved oxygen concentration (in the liquid phase) when it is equilibrated with the gas and $[O_2]$ is its concentration if not at equilibrium. The value of the oxygen transfer constant $k_t$ depends on the volume of the reaction vessel and on the stirring rate. For the experiments done by Degn, Olsen, and Perram,[1] $k_t$ is typically on the order of 0.0035 $s^{-1}$. We shall let $v_{in} = k_t[O_2]_{eq}$ and $v_{out} = k_t[O_2]$. The quantity $v_{in}'$ is taken to be an experimentally controllable parameter since the oxygen pressure can be manipulated. The integration of the system of differential eq 2 was carried out with the Gear method.[22]

**B. Damped and Sustained Oscillations.** Aguda and Clarke[9] reported damped oscillatons in numerical studies of model A but were not able to find sustained oscillations. As shown in Figure 5, we have now determined that model A also generates smooth, almost sinusoidal sustained oscillations using the rate constants given in the figure caption. Calculation of the variation in reaction velocities during the oscillations reveals that the rates of reactions $R_{10}$ and $R_{12}$ oscillate out-of-phase in the same manner as in the YY scheme for the closed system (compare Figures 2 and 6). This implies that the discussion given previously for the YY scheme applies to each period of the sustained oscillations shown in Figure 5.

**C. Bistability between a Steady and an Oscillatory State.** Steady-state analysis of model A shows that a stable oscillatory state and a stable steady state may coexist over certain ranges of the parameters $k_{10}$, $v_{in}$, and $E_t$. For example, we show in Figure 7 an S-shaped curve for the steady state $[O_2]$ as a function of $k_{10}$. In this figure, the two Hopf bifurcation points (labeled H1 and H2) that delineate the boundary of the oscillatory region are shown along with the amplitude of the oscillations indicated by the dotted curve. The positions of the Hopf bifurcation points were determined by numerical calculation of the stability eigenvalues of the steady-state solution; the amplitude of the oscillatory solution which bifurcates from these points was determined from the numerical solutions of the kinetic eq 2. Between the values of $k_{10}$ at H1 and at the lower knee of the S-shaped curve we find the coexistence of a stable oscillatory state and a stable steady state. The coexistence region extends over a range of values of $v_{in}$ and $E_t$ as well; this range will be given in the next subsection.

We show in Figure 8 a simulation of a suggested experiment that could be performed to illustrate bistability between an oscillatory state and a stable steady state. Decreasing the $O_2$ concentration to 0 in the gas phase for a short time (e.g. by setting $v_{in} = v_{out} = 0$) will drive the stable steady state toward a stable oscillatory state (see Figure 8a). On the other hand, if the system

(22) Hindmarsh, A. C.; GEAR: Ordinary Differential Equation Systems Solver, UCID-30001 Rev. 3, Lawrence Livermore Laboratory, December 1974.

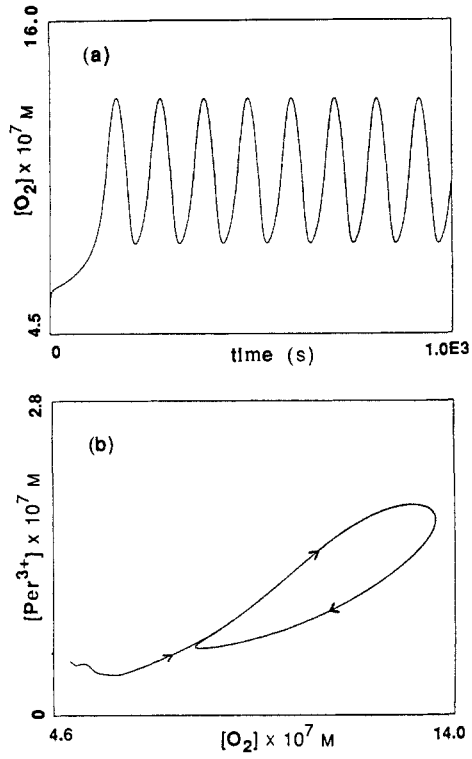


**Figure 5.** (a) Sustained oscillations in oxygen concentration exhibited by model A. (b) A stable limit cycle on the $[Per^{3+}]$–$[O_2]$ plane. Initial conditions (in units of $10^{-7}$ M): $[H_2O_2] = 8.5$, $[NAD^*] = 1.5$, $[O_2^-] = 2.0$, $[O_2] = 5.0$, $[Per^{3+}] = 0.49$, [col] = 80,8, [colI] = 95.0, [colII] = 8.7. Parameters: $k_1 = 1.0 \times 10^7$ $M^{-1}$ $s^{-1}$, $k_2$[NADH] = 1.1626 $s^{-1}$, $k_3$[NADH] = 1.0 $s^{-1}$, $k_8 = 6.0 \times 10^7$ $M^{-1}$ $s^{-1}$, $k_{10} = 1.1 \times 10^9$ $M^{-1}$ $s^{-1}$, $k_{11} = 1.0 \times 10^8$ $M^{-1}$ $s^{-1}$, $k_{12}$[NADH] = 1.0 $s^{-1}$, $k_{13} = 1.0 \times 10^7$ $M^{-1}$ $s^{-1}$, $k_t = 1.0$ $s^{-1}$, and $[O_2]_{eq} = 10^{-5}$ M.

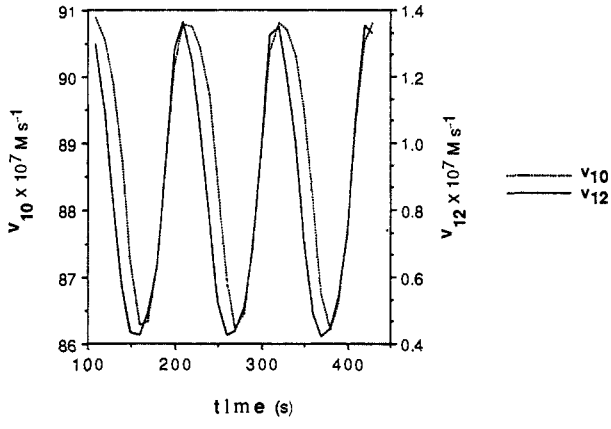


**Figure 6.** Plot of the rates of reactions $R_{10}$ and $R_{12}$ during a few periods of the sustained oscillations shown in Figure 5.

is initially in a stable oscillatory state, a spike of $H_2O_2$ will drive it down to a stable steady state (Figure 8b). Note that the oscillations occur around the higher $O_2$ steady state as predicted by Figure 7. Indeed, such a coexistence of a stable steady state and an oscillatory state has been recently confirmed experimentally by Aguda, Hofmann Frisch, and Olsen.[23]

**D. Phase Diagrams.** The boundary between those parameter values at which a unique steady state exists and those for which three exist is given by the condition that the determinant of the Jacobian matrix must vanish[9]

$$\det [d_x \mathbf{F}] = 0 \tag{5}$$

where $[d_x \mathbf{F}]_{ij} = \partial F_i / \partial X_j$ evaluated at steady state and $\mathbf{F}$ is equal

(23) Aguda, B.; Hofmann Frisch, L.-L.; Olsen, L. F. *J. Am. Chem. Soc.* Submitted for publication.

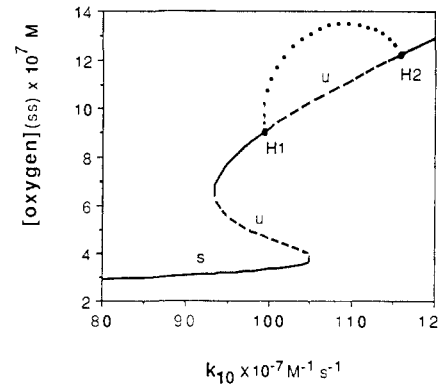


**Figure 7.** Calculated steady states of oxygen as a function of $k_{10}$. Three steady states coexist for values of $k_{10}$ between 93.0 and 105. Between the two Hopf bifurcation points labeled H1 and H2, the steady states are unstable and stable oscillations occur. The amplitudes of these oscillations are schematically shown by the dotted curve (s = stable, u = unstable). Parameter values except $k_{10}$ are given in Figure 5.

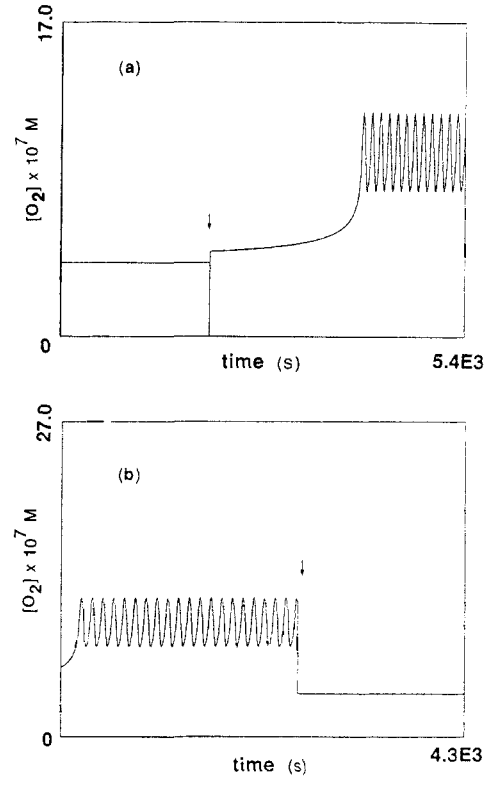


**Figure 8.** (a) A stable steady state is driven to an oscillatory state by cutting off the supply of oxygen for a short time as indicated by the arrow. This is done by letting $k_t = 0$ temporarily for 2 time units during the integration of the kinetic equations. Initial conditions (in units of $10^{-7}$ M): $[H_2O_2] = 4.0$, $[NAD^*] = 3.0$, $[O_2^-] = 7.0$, $[O_2] = 3.7$, $[Per^{3+}] = 0.49$, [col] = 80.8, [colI] = 95.0, [colII] = 8.7. Parameters as in Figure 5 except $k_{10} = 1.05 \times 10^9$ $M^{-1}$ $s^{-1}$. (b) A transition from an oscillatory state to a stable steady state occurs when the reaction system is spiked with $H_2O_2$ at the point indicated by the arrow. The $H_2O_2$ spike is carried out by instantaneously bringing $[H_2O_2]$ up to $4.5 \times 10^{-6}$ M and then continuing the integration. Initial conditions (in units of $10^{-7}$ M): $[H_2O_2] = 8.5$, $[NAD^*] = 1.5$, $[O_2^-] = 2.0$, $[O_2] = 5.0$, $[Per^{3+}] = 0.49$, [col] = 80.8, [colI] = 95.0, [colII] = 8.7. Parameters as in Figure 5 except $k_{10} = 1.05 \times 10^9$ $M^{-1}$ $s^{-1}$.

to the right-hand side of eq 2. The complete and exact steady-state analysis of model A has already been carried out (see eq 5.3 of ref 9). We add here an experimentally useful, mathematically necessary (but not sufficient) condition on the total enzyme concentration for the existence of three steady states:

$$\frac{v_{in}v_{11}}{k_8 k_t} - \frac{k_{12}}{k_{10}} < E_t < \frac{v_{in}}{k_3} + \frac{v_{in}}{k_2} - \frac{k_{12}}{k_{10}} - \frac{k_t k_{13}}{k_{11} k_8} \tag{6}$$

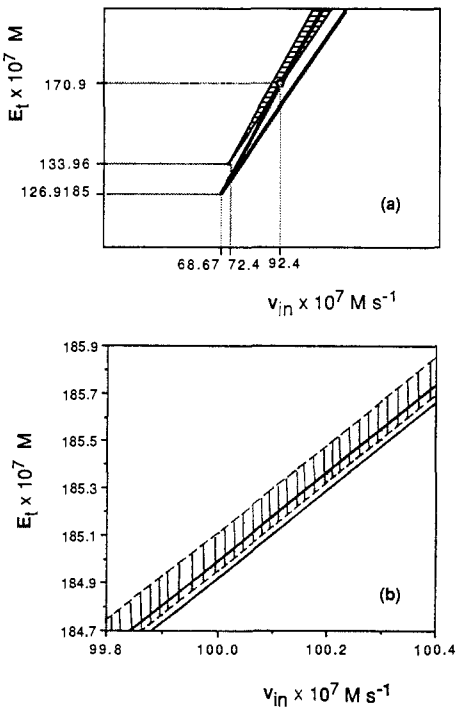


**Figure 9.** (a) Schematic representation of regions of sustained oscillations (hatched) and three steady states (bounded by bold lines) on the $E_t$–$v_{in}$ parameter plane. The widths of these regions have been exaggerated for clarity; the numbers given are numerically determined. All other parameters as in Figure 5 except $k_{10} = 1.05 \times 10^9$ M$^{-1}$ s$^{-1}$. (b) A close-up of the oscillatory (hatched) and multiple steady state (bold lines) regions within a narrow range of $E_t$ and $v_{in}$. A coexistence between a stable oscillatory state and a stable steady state occurs where the two regions overlap.

These inequalities are derived with use of Descartes' rule of signs[24] on the coefficients $\beta_1$ and $\beta_2$ of eq 5.3 of ref 9. The numerically determined region of multiple steady states given in Figure 9 is a subset of the region defined by the inequalities in (6).

The boundary between oscillatory and non-oscillatory regions is given by the Hopf bifurcation theorem[25] which states, among other things, that sustained oscillations will arise when a pair of complex conjugate eigenvalues cross the imaginary axis. In Figure 9, the oscillatory region is plotted along with the three-steady-state region on the $v_{in}$–$E_t$ parameter plane. Again, the parameters $v_{in}$ and $E_t$ are chosen because they are experimentally controllable.

Careful experimental determination of any overlap between the three-steady-state region and the oscillatory region will be necessary to test the prediction of these simulations with model A. We also note, briefly, that variation of a third experimentally adjustable parameter (such as [NADH] which is taken here to be constant) may vary the region of overlap shown in Figure 9. It may be possible to adjust these regions such that the cusp points come close to one another. Such a confluence of degenerate singular points may lead to very exotic dynamics. This possibility is being investigated further in our laboratory.

**E. Different Rate Constants Giving the Same Dynamics.** Before closing this section, we remark on the transformation of the rate constants when one assigns units for concentrations. This transformation affects all rate constants except those of first-order reactions. For example, when one takes the concentrations of $H_2O_2$ and $Per^{3+}$ to be in units of $10^{-7}$ M, the value of the rate constant $k_1$ (in units of M$^{-1}$ s$^{-1}$) will have to be multiplied by $10^7$ to preserve the dynamics of the system. This transformation allows us to map model parameters to experimentally reasonable values of the rate constants. As an explicit example, the rate constants used in Figure 5 were derived from the following unitless parameters, assigning a concentration unit of $10^{-7}$ M: $k_1 = 1.0$, $k_2 = 1.1626$, $k_3 = 1.0$, $k_8 = 6.0$, $k_{10} = 100$, $k_{11} = 10$, $k_{12} = 1.0$, $k_{13} = 1.0$, $v_{in} = 100$, $k_t = 1.0$. These rate constants will give the same sustained oscillations as those used in Figure 5.

Different sets of rate constants giving the same dynamics are found when the kinetic equations are cast in dimensionless form. We report in the Appendix a set of dimensionless equations for model A. Note that the process of de-dimensionalization reduces the number of parameters from 11 to 9. It is also shown in the Appendix that, under oscillatory conditions, the concentrations of the species NAD$^\bullet$ and $Per^{3+}$ are changing at a relatively faster rate compared to those of the other six species. This coincides with our interpretation of the origin of oscillations in this system as being due to switching between autocatalytic production of NAD$^\bullet$ and depletion of this radical by a process that involves $Per^{3+}$.

## IV. Concluding Remarks

The validity of model A can be tested by comparing future experiments to the predictions offered by the computer simulations presented in this paper. One prediction is that of the coexistence of a stable oscillatory state with a stable steady state; more specifically, associated with the oscillatory state is an unstable oxygen steady-state concentration that is higher than the coexisting stable steady state. Aguda, Hofmann Frisch, and Olsen[23] recently found experimental evidence for the coexistence of an oscillatory state with a stable steady state in the peroxidase–oxidase reaction. They also showed that switching between the oscillations and steady state can be accomplished by the oxygen or $H_2O_2$ perturbations predicted by model A.

The only oscillations we have seen so far in our simulations using model A are smooth and almost sinusoidal. The sawtooth-shaped oscillations[2] of both oxygen and NADH seen in most reported experiments at 25 °C have not been generated by simulations with model A (although the 4-species models reproduce this behavior quite well). Fed'kina et al.[16] have presented experimental results which showed that the characteristic phases of compound III kinetics can be identified in each period of the oscillations. Furthermore, when the temperature was increased from 25 to 35 °C (see Figure 3 of ref 16), the abrupt transition between phases was smoothed out and the oscillations became nearly sinusoidal. This variation in temperature would correspond to a variation in rate constants. If the sawtooth and sinusoidal modes do correspond to different temperature ranges, further study of model A with different parameter values should reveal both modes of oscillation.

Other experimentally controllable parameters exist that can be manipulated to give different modes of oscillation. Fed'kina et al.[16] have observed two different kinds of oscillations: (i) a relatively slow reaction with a high $O_2$ concentration and rather low NADH concentration with slow decomposition of compound III (these oscillations have a large period); and (ii) a fast reaction with high NADH concentration and low $O_2$ concentration with

(24) Uspensky, J. V. *Theory of Equations*; McGraw-Hill: New York, 1948.
(25) Hassard, B.; Kazarinoff, N.; Wan, Y-H. *Theory and Applications of Hopf Bifurcation*; Cambridge U.P.: London, 1981.
(26) Chance, B.; Higgins, J. *Arch. Biochem.* **1949**, *22*, 224.
(27) Chance, B. *Arch. Biochem. Biophys.* **1952**, *41*, 416.
(28) George, P. *Biochem. J.* **1953**, *54*, 267.
(29) Dolman, D.; et al. *Can. J. Biochem.* **1975**, *53*, 495.
(30) George, P. *J. Biol. Chem.* **1953**, *201*, 427.
(31) Tamura, M.; Yamazaki, I. *J. Biochem. (Tokyo)* **1972**, *71*, 311.
(32) Yokota, K.; Yamazaki, I. *Biochim. Biophys. Acta* **1965**, *105*, 301.
(33) Wittenberg, J.; et al. *J. Biol. Chem.* **1967**, *242*, 626.
(34) Odajima, T. *Biochim. Biophys. Acta* **1971**, *235*, 52.
(35) Yamazaki, I.; Yokota, K. *Mol. Cell. Biochem.* **1973**, *2*, 39.
(36) Bielski, B.; Gebicki, J. *Biochim. Biophys. Acta* **1974**, *364*, 233.
(37) Odajima, T.; Yamazaki, I. *Biochim. Biophys. Acta* **1972**, *284*, 355.
(38) Rabani, J.; Nielsen, S. *J. Chem. Phys.* **1969**, *73*, 3736.
(39) Yamazaki, I.; Yokota, K.; Tamura, M. In *Hemes and Hemoproteins*; Chance, B., Estabrook, R., Yonetani, T., Ed.; Academic Press: New York, 1966; p 319.
(40) Olsen, L.; Degn, H. *Nature* **1977**, *267*, 177.
(41) Yamazaki, I.; Yokota, K.; Nakajima, R. *Biochem. Biophys. Res. Commun.* **1965**, *21*, 582.

fast decomposition of colII (these oscillations have a small period). The parameters that can be varied in these experiments are the percentage of oxygen in the gaseous mixture, the enzyme concentration, and the NADH concentration in the feed. We have not yet been successful in reproducing the abovementioned modes of oscillation in our computer simulations using model A.

Both model A and the FAB scheme discussed in section IIB assume that NADH concentration is kept constant. In experiments, although NADH must be continuously fed into the reaction system in order to produce sustained oscillations, the NADH concentration in the reactor is seen to undergo oscillations as well. We believe that model A contains the essential network of reactions responsible for the oscillatory behavior of the PO reaction and its ability to exhibit bistability at the same time. Experimentally observed behavior which has not been reproduced by model A includes chaotic oscillations; inclusion of NADH as a time-dependent species may lead to chaos since the variations in the concentration of this species would influence the two feedback loops of model A. It is anticipated that the inclusion of the reactions involving ferroperoxidase, particularly that with oxygen to produce compound 111, could also lead to the complex and chaotic oscillations observed experimentally.

Using values of the parameters in model A (rate constants and total enzyme concentration) used by Yokota and Yamazaki[4] in their nearly quantitative simulation of the closed system via the YY model, we found that only damped oscillations can be generated by model A. These damped oscillations occur only for values of the rate constant for the reaction producing compound 111 that are several orders of magnitude larger than the YY value. What this observation suggests is that a faster production of compound 111 is necessary to produce sustained oscillations; the inclusion of the reaction between ferroperoxidase and oxygen to produce compound 111 ($R_6$ in Table II) is one way to satisfy this requirement and will be studied in future simulations.

**Acknowledgment**. We thank Prof. Lars Olsen of Odense University, Denmark, for keeping us up to date on their experiments with the peroxidase–oxidase reaction. Thanks are also due to Prof. Alexander Scheeline of the University of Illinois at Urbana–Champaign for alerting us to the importance of dimerization of NAD• radicals and the known reactions of the dimer. This research has been supported by NSF Grant CHE-8808191.

## Appendix

We transform the kinetic eq 2 into dimensionless forms which reveals two time scales in the system. Singular perturbation theory[42] treats the dynamics of systems when the dynamical variables have widely differing time scales. For convenience of notation, we let $A = [H_2O_2]$, $B = [NAD^•]$, $C = [O_2^-]$, $F = [O_2]$, $W = [Per^{3+}]$, $X = [coI]$, $Y = [coII]$, and $Z = [coIII]$. Recall that $v_{in} = k_t F_{eq}$.

The dimensionless time and concentrations are

$$\tau = k_t t, \qquad a = \frac{k_1 k_{12}}{k_{10} v_{in}} A, \qquad b = \frac{k_{11}}{k_t} B,$$
$$c = \frac{k_{12}}{v_{in}} C, \qquad f = \frac{k_t}{v_{in}} F = \frac{F}{F_{eq}}, \qquad w = \frac{k_{10}}{k_{12}} W, \tag{A1}$$
$$x = \frac{k_2}{v_{in}} X, \qquad y = \frac{k_3}{v_{in}} Y, \qquad z = \frac{k_8 k_t}{k_{11} v_{in}} Z$$

The corresponding dimensionless parameters are

$$\zeta_a = \frac{k_{10} k_t}{k_1 k_{12}}, \qquad \zeta_b = \frac{k_t^2}{k_{11} v_{in}}, \qquad \zeta_c = \frac{k_t}{k_{12}},$$
$$\zeta_w = \frac{k_{12} k_t}{k_{10} v_{in}}, \qquad \zeta_x = \frac{k_t}{k_2}, \qquad \zeta_y = \frac{k_t}{k_3}, \qquad \zeta_z = \frac{k_{11}}{k_8}, \tag{A2}$$
$$\epsilon = \frac{k_{13} k_t^2}{v_{in} k_{11}^2}$$

The dimensionless dynamical equations are

$$\zeta_a \frac{da}{d\tau} = c - aw$$
$$\zeta_b \frac{db}{d\tau} = c + x + y - bf - bz - 2\epsilon b^2$$
$$\zeta_c \frac{dc}{d\tau} = bf - c - cw$$
$$\frac{df}{d\tau} = 1 - f - bf$$
$$\zeta_w \frac{dw}{d\tau} = y - aw - cw$$
$$\zeta_x \frac{dx}{d\tau} = aw + bz - x$$
$$\zeta_y \frac{dy}{d\tau} = x - y$$
$$\zeta_z \frac{dz}{d\tau} = cw - b \tag{A3}$$

The enzyme conservation constraint is given by the equation

$$\zeta_w w + \zeta_x x + \zeta_y y + \zeta_z z = E_{total}(\text{constant}) \tag{A4}$$

For the values of the rate constants that give sustained oscillations in Figure 5, $\zeta_a = 110$, $\zeta_b = 10^{-3}$, $\zeta_c = 1$, $\zeta_w = 9.09 \times 10^{-5}$, $\zeta_x = 0.6$, $\zeta_y = 1$, $\zeta_z = 1.67$, and $\epsilon = 10^{-4}$. These values imply that $b$ and $w$ (dimensionless concentrations of NAD• and $Per^{3+}$, respectively) are relatively faster variables compared to the other variables.

**Registry No.** NADH, 58-68-4; peroxidase, 9003-99-0.

(42) O'Malley, R. E. *Introduction to Singular Perturbations*; Academic Press: New York, 1974.